Silk degumming time controls horseradish peroxidase-catalyzed hydrogel properties

Journal:	*Biomaterials Science*
Manuscript ID	BM-ART-03-2020-000512.R3
Article Type:	Paper
Date Submitted by the Author:	03-Jun-2020
Complete List of Authors:	Sahoo, Jugal; Tufts University, Biomedical Engineering; University of Strathclyde, Pure and Applied Chemistry Choi, Jaewon; Tufts University, Department of Biomedical Engineering Hasturk, Onur; Tufts University, Department of Biomedical Engineering Laubach, Isabel; Tufts University, Department of Biomedical Engineering Descoteaux, Marc; Tufts University, Department of Biomedical Engineering Mosurkal, Shreyas; Tufts University, Department of Biomedical Engineering Wang, Boyang; Tufts University, Department of Biomedical Engineering Zhang, Nina; Tufts University, Department of Biomedical Engineering Kaplan, David; Tufts University, Department of Biomedical Engineering

ARTICLE

Silk degumming time controls horseradish peroxidase-catalyzed hydrogel properties

Jugal Kishore Sahoo,[a] Jaewon Choi,[a] Onur Hasturk,[a] Isabel Laubach,[a] Marc L. Descoteaux,[a] Shreyas Mosurkal,[a] Boyang Wang,[a] Nina Zhang,[a] David L. Kaplan[a*]

Hydrogels provide promising applications in tissue engineering and regenerative medicine, with silk fibroin (SF) offering biocompatibility, biodegradability and tunable mechanical properties. The molecular weight (MW) distribution of SF chains varies from ~80 to 400 kDa depending on the extraction and purification process utilized to prepare the protein polymer. Here, we report a fundamental study on the effect of different silk degumming (extraction) time (DT) on biomaterial properties of enzymatically crosslinked hydrogels, including secondary structure, mechanical stiffness, *in vitro* degradation, swelling/contraction, optical transparency and cell behaviour. The results indicate that DT plays a crucial role in determining material properties of the hydrogel; decrease in DT increases β-sheet (crystal) formation and mechanical stiffness while decreasing degradation rate and optical transparency. The findings on the relationships between properties of silk hydrogels and DT should facilitate the more rational design of silk-based hydrogel biomaterials to match properties needed for diverse purpose in biomedical engineering.

Introduction

Hydrogels are three-dimensional (3D) networks of polymers that can retain substantial amounts of water, while maintaining structural integrity due to chemical or physical crosslinked networks. Since their introduction in the 1950s, hydrogels of synthetic or natural polymers have attracted attention in the fields of delivery of drugs,[1, 2] cells,[3] tissue engineering[4, 5] and regenerative medicine[6, 7] due to their physical, chemical and mechanical properties. Significant progress has been made towards the design and development of functional hydrogel systems based on different synthetic polymers, including poly(ethyleneglycol) (PEG), poly(N-isopropylacrylamide)(PNIPAm) and poly(2-hydroxyethyl methacrylate) (pHEMA),[8, 9] as well as natural polymers, such as silk fibroin, elastin, alginate, hyaluronic acid and resilin.[10-12] While the use of synthetic polymers provides advantages, such as a high degree of control over properties (e.g., hydrophilic-hydrophobic balance and mechanical strength), and reproducibility in polymer preparations,[13, 14] synthetic materials typically have limitations in terms of cell affinity (lacking biological recognition sites) and can lead to degradation products that result in inflammation.[15] In this regard, natural biopolymers are interesting, as they biodegrade into metabolically useful components, and can provide biological recognition sites.[16-18]

Silk fibroin (SF), a biopolymer derived from the cocoons of domesticated *Bombyx mori* silkworms, provides biocompatibility, biodegradability, robust mechanical strength and flexible processability.[19-22] These properties make SF-based hydrogels appealing scaffolds for various biomedical applications. SF hydrogels can be prepared by physical crosslinking through vortexing,[23] sonication,[24, 25] changes in pH[26] or temperature[27] and γ-ray irradiation.[28] In addition to physical crosslinking, enzymatic crosslinking mediated by horseradish peroxidase (HRP) in the presence of hydrogen peroxide (H_2O_2) to form silk hydrogels has been reported. [29, 30] In the presence of H_2O_2, HRP mediates the formation of tyrosyl free-radicals [31] that react to primarily form covalent dityrosine crosslinks.[32] HRP reacts with H_2O_2 to form an intermediate compound consisting of an oxyferryl center and a porphyrin based cation radical. The activated HRP then subjected to two single electron oxidation reactions in presence of tyrosine to form tyrosyl free radical, which can couple with an adjacent tyrosyl radical in the same or different silk chain to form dityrosine bond.[29, 32] HRP-mediated dityrosine crosslinking leads to the formation of SF hydrogel networks that were mechanically tunable, optically transparent, biodegradable, and supported cell survival and proliferation, making them applicable for tissue engineering and regenerative medicine.[29, 33-35] Generally, the molecular weight (MW) of polymers is a key factor that dictates hydrogel properties, such as stiffness, swelling ratio, secondary structure formation and degradation kinetics.[36-39] In case of SF, the DT controls the MW, i.e. higher DT results in lower SF MW and vice versa. SF MW influences the gelation kinetics of enzymatically crosslinked SF hydrogels[40] but the influence on material properties has not been investigated. This is in contrast to other biopolymers such as hyaluronic acid,[36] alginate,[39] and chitosan,[41] where hydrogel properties have been correlated with MW. The effect of MW on electrospinning using

a. *Department of Biomedical Engineering, Tufts University, 4 Colby St, Medford, MA, 02155*

regenerated SF has been reported.[42] Further, the effect of MW on different physical properties of SF hydrogels prepared by ultra-sonication has been investigated,[43] where the silk chains were physically crosslinked. However, there has been no report on the effect of DT on different biomaterial properties of enzymatically crosslinked SF hydrogels. Enzyme-catalyzed hydrogels provide certain advantages over physically crosslinked silk hydrogels as they can provide tunable control of gel properties in physiological conditions, elastomeric behavior and optical clarity.[44] In physically crosslinked SF hydrogels, β-sheets crystals are responsible for the crosslinks, thus higher stiffness when compared to the enzymatic counterparts.[29]

The aim of the present study was to systematically investigate the effect of silk DT on the material and biological characteristics of enzymatically crosslinked SF hydrogels. Different DTs of 1, 30 and 120 minutes produce three different MW distributions with peak MWs of 391 kDa (high), 157 kDa (medium) and 79 kDa (low) respectively. Aqueous solutions of SF were enzymatically crosslinked in the presence of HRP and H_2O_2 to form hydrogels. Different material properties such as β-sheet content, dityrosine formation, enzymatic degradation, mechanical properties, optical transparency, swelling/contraction, and cytocompatibility were investigated. The results showed that with decreasing DT, the crystalline β-sheet content and stiffness of the hydrogels increase, while optical transparency and the rate of enzymatic degradation decreased. All hydrogel formulations introduced in the present study supported cell growth, suggesting that enzymatically crosslinked SF hydrogels offer cytocompatible systems across a wide range of MWs. These findings may aid the rational design of SF hydrogels, as well as with respect to other silk-based biomaterial formats for different biomedical applications.
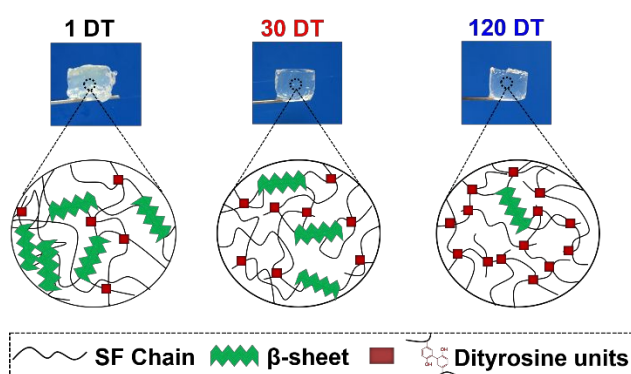
Scheme 1: Scheme depicting the effect of DT on the enzymatic crosslinking of SF hydrogels in the presence of HRP and H_2O_2. All MWs formed into hydrogels, while the content of chemical crosslinks and crystals varied, impacting the properties of the different hydrogels formed in these reactions.

Results and Discussions

Regenerated silk solutions were prepared from *Bombyx mori* silkworm cocoons following procedures reported previously.[45]

Briefly, fibroin protein was extracted from cocoons after degumming in 0.02M sodium carbonate. The MW distribution of SF protein fragment depended on the DT.[46] Three different MW distributions of SF were achieved by extracting the cocoons for 1, 30 or 120 minutes. The MW distribution of SF was digitally quantified on polyacrylamide gel images after polyacrylamide gel electrophoresis (PAGE) (**Figure S1,2**). Using the calibration curves of log MW versus distance from the wells in pixels, the frequencies of each MW were determined. The MW with highest frequency for 1, 30- and 120-minutes DT were 391, 157, and 79 kDa, respectively, while the mean MWs were 146, 77 and 69 kDa, respectively. (**Figure S1, 2**). The composition of the raw silkworm cocoon includes 20-30 wt% sericin, a glue-like protein coating with molecular weights ranging from 20 to 400 kDa.[47] The complete removal of sericin through degumming by extraction in ~0.02 M Na_2CO_3 solution should require ~30 minutes.[48] It is also reported that 5 minutes degummed silk contain <10 wt% of sericin.[47] For the 1 minute-extracted regenerated silk solutions, the quantity of residual sericin could be higher than that of 5 minutes extracted silk and lower than that of raw fibers. Thus, the MW could be due to the contributions from both fibroin and residual sericin protein. Residual silk sericin is known to effect the structure and properties of regenerated silk due to different amino acid composition.[49, 50] Sericin is more hydrophilic than SF as it has significantly higher contents of charged acidic (~24 mol%) and basic (~6 mol%) amino acids [51] in comparison to fibroin (1.1 and 0.6%, respectively) [50] However, The tyrosine content of sericin (~3 mol%) is lower than fibroin (~5 mol%). Therefore, residual sericin present in 1 DT silk might affect its hydrogel properties. Silk solutions were characterized by ^{1}H-NMR spectroscopy (**Figure S3-5**) to confirm the major amino acid compositions in the various silk preparations.

Silk hydrogels were then prepared by mixing aqueous SF solutions in ultrapure water with HRP and H_2O_2 to initiate the formation of phenolic radicals on the tyrosine residues in the silk (~5% of the amino acids), which could form intra- or inter-chain dityrosine bond via condensation of the phenolic rings.[32] To investigate the relationship between DT and material properties, the experiments were designed with same reaction conditions i.e. same SF (2.5% w/v), HRP (10 U/mL) and H_2O_2 (2.4 mM/mL) concentrations while the DT of silk was the only variant.

Time-dependent hydrogel stiffening was previously observed when these crosslinked hydrogels were incubated in PBS and cell culture media, due to the increase in their β-sheet content.[52] The gradual increase in stiffness is an important material property recognized by cells through mechanotransduction, which impacts biological properties such as cell proliferation, morphology and lineage commitment.[35] Control of this time-dependent stiffening of enzymatically crosslinked hydrogels was also demonstrated before by controlling the concentrations of SF and H_2O_2.[29, 30, 52] To investigate the role of DT on the modulation of β-sheet content and changes in hydrogel stiffness over time, the hydrogels of different DTs were incubated in 1X PBS at 37 °C for 7 days. Changes in

secondary structure profiles were analysed using attenuated total reflectance-Fourier transform infrared spectroscopy (ATR-FTIR) in the amide I region (1700-1600 cm^{-1}).
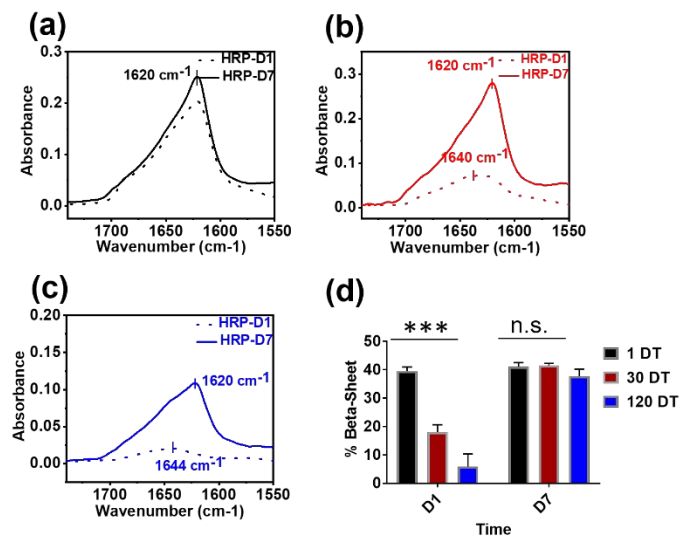
Figure 1: Representative ATR-FTIR spectra of hydrogels of different silk DT crosslinked in the presence of HRP/H$_2$O$_2$. D1 and D7 samples were incubated in 1X PBS (phosphate buffered saline) for 1 and 7 days, respectively, after hydrogelation. a, b, c) Time-dependent FTIR spectra for 1, 30 and 120 DT silk hydrogels, respectively. For D7, all samples showed strong β-sheet absorption band at 1620 cm^{-1}. However, at D1, low DT (1 DT) showed strong β-sheet absorption bands whereas higher DT silk (30 and 120 DT) showed weak absorption bands. d) Percentage β-sheet content in the hydrogels increased with time after incubation in PBS at 37°C. (data are presented at mean ± standard deviation; n=3, ***p < 0.001 by two-way ANOVA with Tukey's post hoc test)

The FTIR bands at 1637-1616 cm^{-1} and 1655-1638 cm^{-1} are associated with β-sheet structures and random coils, respectively.[53] From D1 to 7, no significant difference was recorded in the absorption spectrum of the 1 DT hydrogels, which displayed a strong peak at 1620 cm^{-1} (**Figure 1a**). For the high DT hydrogels, in contrast, a significant band shift from 1644 cm^{-1} to 1620 cm^{-1} was observed over the seven days, suggesting a conformational change of SF from random coil to β-sheet structure (**Figure 1 b, c**). At D1, the β-sheet content of 1, 30 and 120 DT silk hydrogels were 39.5 ± 1.47%, 18 ±2.57% and 5.9 ±4.50%, respectively (**Figure 1d**), suggesting that the initial crystalline content increased significantly with decreasing DT over time in PBS, At D7, the β-sheet contents were 41.1 ± 1.49%, 41.5 ± 0.78, 37.7 ± 2.51% for 1, 30 and 120 DT, respectively, with no significant difference among the groups (**Figure 1d**). These observations indicated that there was no significant change in the crystalline content of low DT (391 kDa) SF hydrogels in physiological buffer over time, while a substantial increase occurred for higher DT (157 and 79 kDa) hydrogels. The high initial β-sheet content of the 1 DT hydrogels could be related to the longer SF chains with lower chain mobility, favoring thermodynamically driven self-assembly through interactions between hydrophobic domains in the SF sequence. Taken together,

the results indicate that DT of SF significantly influences secondary structure in enzymatically crosslinked silk hydrogels.

The effect of DT of silk fibroin on dityrosine formation in the hydrogels was investigated using liquid chromatography tandem mass spectroscopy (LC-MS/MS) after 24h of the reactions. **Figure 2a**
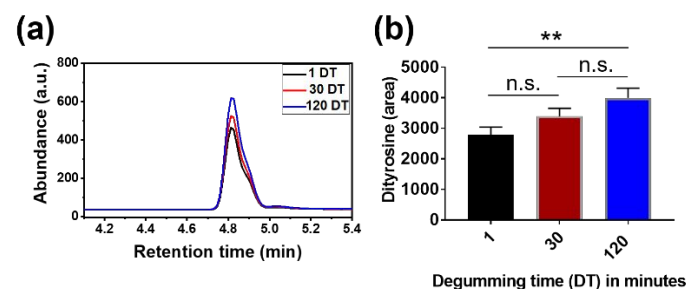
Figure 2: Analysis of dityrosine bonds using LC-MS/MS analysis. (a) LC-MS/MS chromatograms obtained from analysis of silk hydrogels formed with 1 DT (black), 30 DT (red), and 120 DT (blue) samples, where the concentration of the silk solutions was fixed at 2.5% w/v. (b) Relative peak area of dityrosine in peak area in the hydrogels, as compared within the sample groups based on the peak areas (data are presented as mean ± standard deviation; n = 3, **p < 0.01 by one-way ANOVA with Tukey's post hoc test).

shows the chromatograms of the hydrogels produced by different SF with different DTs. Product ions for dityrosine (m/z transition = 361.1 → 315.3) were identified, where the typical retention time was 4.8 minutes. (**Figure S6**) The relative peak area of dityrosine between the three samples was as follows: the 1 DT sample had the lowest value of 2,788 ± 249, the 30 DT samples had a value of 3,398 ± 257, and the 120 DT samples had the highest value of 3,992 ± 322, where a statistically significant difference was observed between the 1 and 120 DT samples (**Figure 2b).** These results indicated that dityrosine formation in the hydrogels increased as the DT of SF increased. This trend can be explained by the viscosity of the silk solutions, which were determined by the concentration and MW of SF.[42, 54] Since the concentration of the silk solution was held constant in all experiments, longer chain lengths of SF molecules resulted in higher degrees of the chain entanglement, leading to increased viscosity of the solution. In this case, the collisions between phenolic radicals produced by HRP-catalysed reactions could be more limited due to this lower chain mobility of SF molecules, resulting in lower dityrosine bond content.[55] As a result, the lowest abundance of dityrosine was found in the hydrogels prepared using 1 DT silk.

The mechanical properties of hydrogels were assessed using unconfined compression tests, where the preformed hydrogels were immersed in PBS at 37°C and analyzed on D1 after synthesis. The compressive mechanical properties of silk hydrogels produced by HRP-mediated crosslinking reactions were significantly influenced by the DT of silk (**Figure 3**). For compressive loading and unloading cycles to 30% strain (**Figure 3a**), the hydrogels formed with 1 DT (lowest DT) showed the largest hysteresis, indicating that the hydrogel did not return to its original state when the applied force was removed, due to the energy absorbed by plastic

deformation.[56] However, there was a decrease in hysteresis as the DT of silk was increased, so that the hydrogels formed with 120 DT exhibited the smallest hysteresis with very high resilience (**Figure 3a**). As shown in **Figure 3b**, the energy loss of the hydrogels for a single cycle was 72.9 ± 13.7, 26.1 ± 3.9, and 21.2 ± 4.5 % for 1, 30, and 120 DT, respectively, which decreased as the DT of silk increased. Significant differences
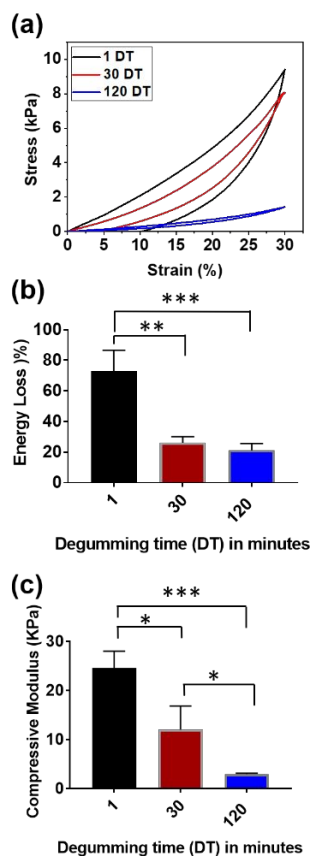
Figure 3: Compressive mechanical properties of silk hydrogels after 24h of hydrogel formation. (a) Representative compressive stress-strain curves for 1 DT (black), 30 DT (red), and 120 DT (blue) samples. (b) Energy loss calculated from the area between the loading and unloading in the stress-strain curve. (c) Compressive modulus of hydrogels. (data are presented as mean ± standard deviation; n = 3, *p<0.05, **p < 0.01 and ***p < 0.001 by one-way ANOVA with Tukey's post hoc test).

between 1 and 30 DT and between 1 and 120 DT were observed, suggesting that the low DT of silk significantly affected the increase of energy loss of the hydrogels. This could be attributed to the formation of heterogeneous hydrogel networks caused by fast gelation with the 1 DT samples. In this case, when the compressive force was applied, the redistribution of stress throughout the heterogeneous hydrogel networks caused rapid stress concentration into weaker mechanical areas or structural defects, resulting in plastic deformation.[57] Additionally, a significantly higher β-sheet content of the hydrogels formed with the 1 DT samples (**Figure 1** at D1) when compared to the hydrogels formed with 30 and 120 DT. This result influenced the inelastic and stiff properties of the hydrogels. The compressive moduli of the hydrogels formed

with 1, 30, and 120 DT were 24.6 ± 3.5, 12.0 ± 4.8, and 3.0 ± 0.2 kPa, respectively (**Figure 3c**), where the modulus decreased significantly with increasing DT of SF.

SF degrades *in vitro* and *in vivo* in the presence of different proteolytic enzymes (e.g. protease XIV, α-chymotrypsin, proteinase K, collagenase).[16] Control over degradation kinetics is an important parameter for tissue regeneration, for release of biochemical agents
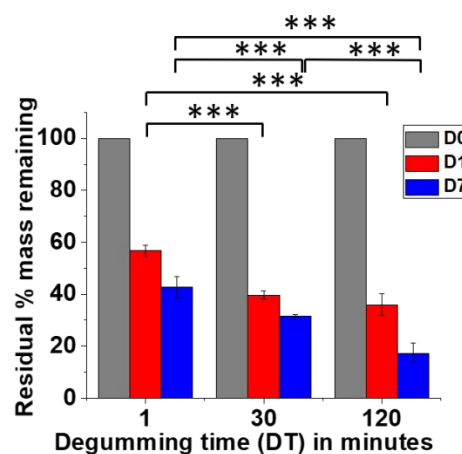
Figure 4: *In vitro* enzymatic degradation of silk hydrogels of different DT over 7 days of incubation in 1X PBS with 0.001 U/mL chymotrypsin. Data at D1 and D7 are presented as residual percentage mass remaining of D0. Data are presented as mean ± standard deviation; n = 3, **p < 0.01 and ***p < 0.001 by two-way ANOVA with Tukey's post hoc test.

and for medical devices in general.[20, 21, 58] Enzymatic degradation of SF leads to the breakdown of silk chains into peptides and eventually amino acids. α-Chymotrypsin and protease XIV facilitate efficient degradation.[16]

Silk protein generally has slower degradation rates in comparison to other natural biopolymers such as hyaluronic acid, collagen, gelatin and elastin due to the resistant beta sheet crystals.[17] To understand the effect of DT on enzymatic degradation, hydrogel discs of the different DTs were incubated in α-chymotrypsin (0.001 U/mL in 1X PBS) and monitored for 7 days at different times (D1, D7) for insights into degradation kinetics. At D1, 391, 157 and 79 kDa MW SF degraded 43%, 60% and 64 % while at D7, they degraded 57%, 68% and 83% of original mass, respectively (**Figure 4**). The degradation kinetics were slower for silk hydrogels with decreasing DT. Since the variables for hydrogel formation (silk, HRP, and H_2O_2 concentrations) were fixed except for DT, SF hydrogel degradation depended on the DT and was reflected in the crosslinking discussed earlier. At D1, slower degradation for 391 kDa MW SF (lowest DT) can be related to higher β-sheet content (**Figure 1D**) which limits accessibility and diffusivity of the enzyme to the silk chains.[35]

(a)

(b)

% swelling by mass			
	1 DT	**30 DT**	**120 DT**
1h	25.0	31.3	304.9
2h	26.7	45.7	627.9
24h	12.4	29.4	857.8

% contraction by mass			
	1 DT	**30 DT**	**120 DT**
1h	34.3	41.2	9.2
2h	49.7	51.7	16.0
24h	50.5	63.2	34.9
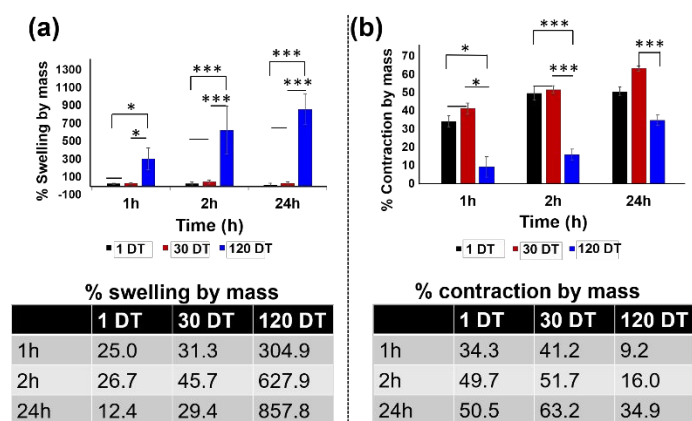
Figure 5: Investigation into swelling (a) and deswelling (contraction) (b) of different DT SF hydrogels in ultrapure water and 1X PBS, respectively. The Table under each figure corresponds to percent swelling and deswelling by mass at different time intervals (1h, 2h, 24h) for the different MW SFs. Data are presented as mean ± standard deviation; n = 3, *p<0.05, **p < 0.01 and ***p < 0.001 by two-way ANOVA with Tukey test).

The properties of hydrogels in terms of swelling and contraction in response to different environmental changes can be leveraged to design materials for controlled and targeted drug-delivery.[59] Hydrogel swelling and contraction behavior is influenced by a number of factors such as pH, temperature, ionic strength of the medium, crosslinking density, and hydrophobicity/hydrophilicity.[60-63] To investigate the effect of DT on swelling and contraction properties of the SF hydrogels, hydrogel discs were immersed in ultrapure water (for swelling) and in 1X PBS (for contraction) and monitored over 24h (**Figure 5**). The different MW SFs swelled differentially in water (**Figure 5a**) and high DT SF (79 kDa) swelled a maximum of 305% of the original mass after 1h. For low MW SF (79 kDa), the swelling increased at 24h, to 858% of the original mass (**Figure 5a, Figure S8**). However, for the SF with lower DTs (391 and 157 kDa), although there was an increase in swelling at 2h, the decrease in swelling after 24h was unclear. The maximum percent swelling for the higher DT SF (79 kDa) could be attributed to the weak network (low β-sheet content and compressive modulus (**Figure 1d, 3c**) with room to absorb more water.[43]

Like the swelling behavior, the DT of silk also influenced hydrogel contraction in 1X PBS at pH 7.1. The hydrogel with higher DT showed the smallest percent contraction over 24h (**Figure 5b**). After 24h, the 1, 30 and 120 DT hydrogels contracted by 51, 63 and 35 % of their original masses, respectively, with no statistically significant difference between the 1 and 30 DT groups at any time point. The contraction of SF hydrogels in PBS could be explained with salting out effects in the relatively high ionic strength buffer rich in sodium and potassium ions, which can induce the self-assembly of SF chains and hydrogel stiffening through the removal of the hydration layers around the hydrophobic domains.[64-66] The lower contraction with increasing DT could be explained with the higher content of hydrophilic free N- and C-termini in the high DT SF with shorter chains, due to more random cleavage of the SF chains as a result of the longer extraction times.

(a)

(b)

(c)
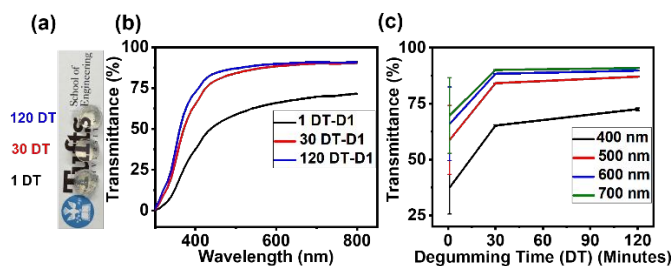
Figure 6: (a) Digital images of silk hydrogels formed from different DT. Appearance of the bottom letters depicts the macroscopic transparency of each MW hydrogel after 24h. The hydrogels were prepared in a PDMS mold. (b) Percent transmittance of SF hydrogels at different wavelengths measured after 24h. (c) Percent transmittance of SF hydrogels at different wavelengths. Data are presented as mean ± standard deviation; n = 3.

The optically transparency of hydrogels provides opportunities for applications in vitreous substitutions[33] and cornea replacements, among other areas of utility.[67] To investigate the effect of DT on optical properties of different SF hydrogels, the transmittance in visible light was measured after 24h. Interestingly, we observed that hydrogels prepared with different DT exhibit different light transmittance at different wavelengths (**Figure 6b, c**). The transmittance at visible light wavelengths (400-700 nm) was calculated and plotted against SF DT (**Figure 6c**). Transmittance increased with increase in wavelength for all MWs and decreased with decrease in DT. The optical transparency was highest at 700 nm for all hydrogels and the mean percent transmittance was 69.7, 90.1 and 91% for 1, 30 and 120 DT, respectively. Crystallinity plays an important role affecting the transparency of SF hydrogels.[68] As described above in **Figure 1D**, β-sheet content was highest in the low DT hydrogels at D1, indicating the different β-sheet contents in different DT hydrogels influenced optical transparency[43], with higher β-sheet content resulting in lower transparency and vice versa. Also, it should be noted that the heterogeneous microstructures induced by β-sheet crystallinity are also related to the optical transmittance of the hydrogels.[68] If the cluster size of heterogeneous microstructures is smaller than the wavelength of visible light, the hydrogel is transparent, while the hydrogels become opaque when these clusters are larger.[43] Therefore, the hydrogels with lower DT likely formed larger sized clusters (due to the longer SF chains) of heterogeneous microstructures resulting in light scattering in the visible light wavelength range (400-700 nm). While no color change of the hydrogels prepared from different DT SF was visually observed, the oxidation of the phenol (i.e., tyrosine residues) generally results in color formation due to the generation of quinone-type intermediates.[69-72] This color formation can be determined by monitoring the absorbance at 455 nm.[73] From the transmittance at 455 nm (**Figure 6b**), therefore, it is speculated that the hydrogels with lower DT could include more quinone-type intermediates generated by HRP-mediated reactions, leading to decreased transmittance.

To investigate the influence of SF DT on the behavior of adherent cells, murine L929 fibroblasts were cultured on the hydrogel surfaces and their viability, morphology and metabolic activity were

monitored over 8 days. Cells attached and proliferated on all hydrogel surfaces (**Figure 7a**) and cell viability was over 90% at D1 (**Figure 7b**), suggesting cytocompatibility of the SF hydrogels irrespective of DT. However, significant differences were observed in initial cell morphology at D1 and metabolic activity over 8 days. The cells on the 30 DT hydrogels had higher spread area/lower circularity at D1 (**Figure S9**) and a slightly higher fold increase in metabolic activity over 8 days (**Figure 7c**) than those on the 120 DT

silk hydrogels. This could be explained with 30 DT silk gels having a higher initial stiffness (~10 kPa vs. ~2 kPa of 120 DT hydrogels), which was shown before to improve spreading, filopodia formation and proliferation of fibroblasts,[74, 75] likely through actinmyosin-
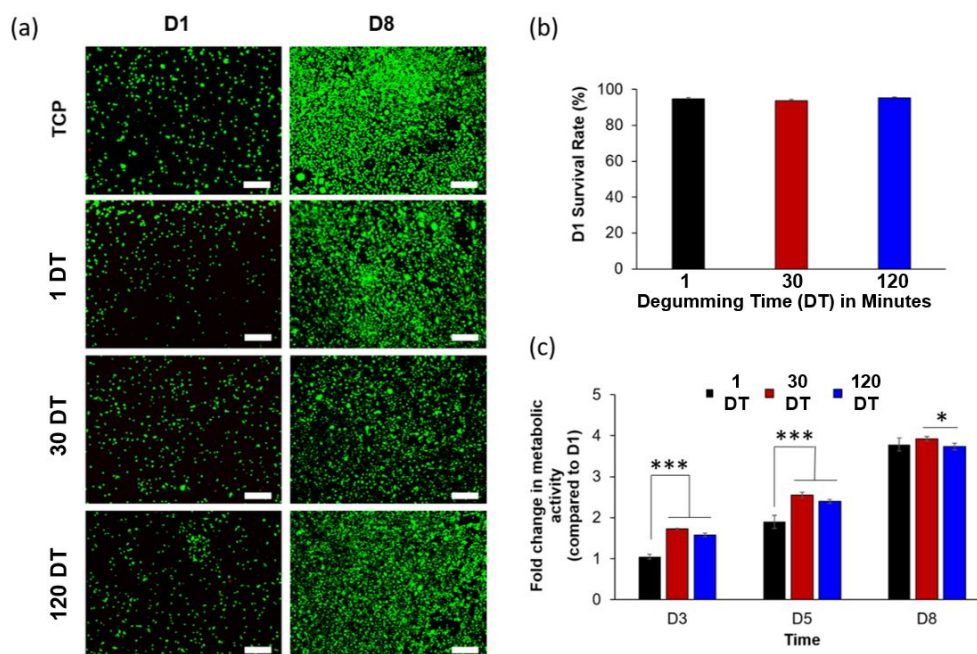
Figure 7: Cytocompatibility of the hydrogels. (a) Fluorescent micrographs of Live/Dead stained L929 fibroblasts cultured on the SF hydrogels. Green: calcein (live), red: EthD-1(dead), scale bars: 200 μm. (b) Survival rates of the cells at day 1. (c) Fold changes in metabolic activity of the cells cultured on hydrogel surfaces compared to day 1. (n = 4, *$p < 0.05$, **$p < 0.01$ and ***$p < 0.001$).

dependent mechanosensing that regulates gene expression and cell fate.[76] Interestingly, the cells on the 1 DT silk hydrogels, the stiffest (~25 kPa) substrate starting from D1, had a spherical morphology with the lowest initial spread area and fold increase in metabolic activity at D3 and D5. Moreover, the 1 DT silk samples that were degummed for only 1 minute may contain residual sericin, which has shown to improve cell attachment, spreading and proliferation on SF-based materials.[77-79] Even though the fold change in metabolic activity on the 1 DT hydrogels leveled up with the other groups at D8, the percent dye reduction was significantly lower than those on the 30 and 120 DT counterparts at all time points (**Figure S10**), indicating lower metabolic activity. Inferior cell spreading and metabolic activity on the 1 DT hydrogels despite high stiffness and possibly residual sericin could be because of lower free C-terminus carboxylic acid and N-terminus primary amine content compared to the 30 and 120 DT hydrogels. This might have influenced the amount, type and conformation of the adsorbed proteins from the media[80] and in turn, affected cell behavior, considering that spreading and proliferation of adherent cells were reported to be improved significantly with increasing hydrophilicity[81, 82] or carboxylic acid and primary amine residues on the substrate surfaces.[83]

Conclusions

In this study, we assessed the effect of DT on biomaterial properties of enzymatically crosslinked SF hydrogels and found that DT was a critical parameter for the design and development of enzymatically crosslinked silk-based hydrogels for different applications. The DT plays a key role in controlling hydrogel properties such as β-sheet formation, dityrosine bond formation, mechanical stiffness, *in vitro* degradation, swelling/contraction, transparency, and cell behavior. In summary, lower DT promoted more β-sheet content, lower dityrosine formation, higher stiffness, slower degradation, less swelling and less transparency. The enzymatic hydrogels described here have been applied in a number of fields including tissue engineering, cell encapsulation and vitreous applications to demonstrate their versatility.[29, 33, 35] We expect these new findings on DT-property relationships will facilitate the rational engineering of enzymatically crosslinked silk-based hydrogels, enabling further advancement of these systems in various biomedical applications.

Materials and Methods

All materials and commercial reagents were used as purchased. All solvents were used as supplied (analytical or HPLC grade) without further purification.

Experimental Procedures

Preparation of aqueous silk solution: Silk fibroin solutions were prepared using our previously reported procedures.[45] Briefly, 5 grams of *B. mori* silkworm cocoons were cut into small pieces and boiled (extracted) in 2 L of 0.02 M Na_2CO_3 solution (Sigma-Aldrich, St. Louis, MO) in a glass beaker for 1, 30 and 120 minutes separately, subsequently referred to as 1, 30 and 120 DT respectively, to remove the sericin protein coating. Degummed fibers were collected and rinsed with distilled water three times, followed by air-drying in a fume hood overnight. Next day, the degummed fibers were solubilized in 9.3 M LiBr (Sigma-Aldrich, St. Louis, MO) in a pre-heated oven at 60°C for 4h (6h for 1 minute boiled). After 4h, a light brown color SF solution was obtained which was then dialyzed against 4L of deionized water (water changes after 1, 2, 4, 24, 36, and 48 h) with a dialysis tube (3,500 MWCO, Thermo Scientific, Rockford, IL). The purified silk protein solution was then centrifuged twice (9,000 RPM, 20 min, 4°C) to remove insoluble white/brown aggregates. SF concentration was determined by drying a known mass of the silk solution in an oven at 60°C overnight and assessing the mass of the remaining solid film.

Preparation of HRP crosslinked SF hydrogels: Horseradish peroxidase (HRP), type VI (Sigma-Aldrich, St. Louis, MO) lyophilized powder was dissolved with distilled water to form a stock solution with a concentration of 1000 U mL^{-1}. The HRP solution was added to the SF solution of different DTs (1, 30 and 120 DT), in a ratio of 10 U of HRP to 1 mL of silk solution. To initiate gelation, 10 µL of 243 mM of freshly prepared hydrogen peroxide (Sigma Aldrich, St. Louis, MO) solution were added per mL of silk solution, for a final concentration of 2.43 mM, and mixed by gentle pipetting prior to setting. The final SF concentration used for gelation was 2.5% w/v. The solution was incubated at 37°C for 4h before analysis.

PAGE (Polyacrylamide gel electrophoresis) analysis of SF: In order to determine the molecular weight of silk fibroin (high molecular weight, 1 minute extracted) solution, Tris-acetate gel was run in a gel electrophoresis chamber. Gel electrophoresis was performed in three steps:

1) **Sample preparation**: 1 wt% of the SF solutions were prepared. In an Eppendorf, 25 µL of the SF was mixed with 65 µL of LDS sample buffer (Invitrogen, NuPAGE, Lot: 2020067) and 10 µL of reducing agent. The solutions were mixed well and heated at 70°C (pre-heated digital dry heat bath (Model: BSH1002, USA Scientific, Ocala, FL)) for 10 minutes.

2) **Sample loading**: In a gel electrophoresis chamber, 10 µL of the samples were loaded into the well along with the reference ladder (Invitrogen, HiMark™ Pre-Stained Protein Standard (Lot 2028200). Gels were run at 150 V for 1h in 1X tris-acetate running buffer.

3) **Staining**: After 1h, the gel was removed and transferred to a Petri dish. Colloidal blue stain (55 ml DI water, 20 mL methanol, 5 mL of stain B (Invitrogen, NOVEX, Stainer B, Colloidal Blue Stain Kit, Part No: 46-7016, Lot no: 2030143), 20 mL stain A (Invitrogen, NOVEX, Stainer A, Colloidal Blue Stain Kit, Part No: 46-7015, Lot no: 2030142)) was prepared and the gel was immersed in the stain with gentle shaking for 3h at room temperature. After 3h, the stain was removed, and the gel was rinsed in DI water multiple times before washing the gel in DI water for a final washing overnight. The next day, DI water was removed from the petri dish and the gel was imaged.

To determine the molecular weight of silk fibroin (lower molecular weight, 30 and 120 minutes extracted) solution, bis-tris-acetate gel was run in a gel electrophoresis chamber. Gel electrophoresis was performed in three steps:

1) **Sample preparation**: 1 wt% of the SF solutions were prepared. In an Eppendorf, 25 µL of the SF was mixed with 65 µL of LDS sample buffer (Invitrogen, NuPAGE, Lot: 2020067) and 10 µL of reducing agent. The solutions were mixed well and heated at 70°C (pre-heated digital dry heat bath (Model: BSH1002, USA Scientific, Ocala, FL)) for 10 minutes.

2) **Sample loading**: In a gel electrophoresis chamber, 10 µL of the samples were loaded into the wells along with the reference ladder (Invitrogen, NOVEX sharp- pre-Stained Protein Standard (Lot 2066829). Gels were run at 200 V for 30 minutes in 1X MES (2-(N-morpholino) ethanesulfonic acid) running buffer.

3) **Staining**: After 30 minutes, the gel was transferred to a Petri dish. Staining was performed in two steps. I) Fixing solution was prepared by mixing100 mL methanol, 20 mL acetic acid and 80 mL of DI water. Colloidal blue stain (55 ml DI water, 20 mL methanol, 20 mL stain A (Invitrogen, NOVEX, Stainer A, Colloidal Blue Stain Kit, Part No: 46-7015, Lot no: 2030142)) was prepared as staining solution. At first, the gel was immersed in the fixing solution for 10 minutes while rotating in a shaker. After 10 minutes, the fixing solution was removed, and staining solution was added and shaken at RT for 10 minutes. After 10 minutes, 5 mL of stain B (Invitrogen, NOVEX, Stainer B, Colloidal Blue Stain Kit, Part No: 46-7016, Lot no: 2030143) was added with gentle shaking for 3h at room temperature. After 3h, the stain was removed, and the gel was rinsed in DI water multiple times before washing the gel in DI water for a final washing overnight. The next day, DI water was removed from the petri dish and the gel was imaged.

The molecular weight distributions of silk fibroin were determined using ImageJ software. Briefly, the distance in pixels from the well on each lane was converted to a molecular weight value using the equation obtained from the calibration curve prepared by the analysis of mean grey values on the reference ladder lanes (**Figure S4 and 5**). Then, mean grey values on each sample lane were converted to frequency of each molecular weight in the protein smears to plot molecular weight distributions of the samples. The mean molecular weight and the molecular weight with the highest frequency were determined from these distributions and reported.

Fourier transform infra-red (FT-IR) spectroscopy: Protein secondary structures of HRP hydrogels were determined using a JASCO FTIR 6200 spectrometer (JASCO, Tokyo, Japan) with a MIRacle attenuated total reflectance (ATR) with germanium crystal. Data were obtained by averaging 32 scans with a resolution of 4 cm^{-1} within the wavenumber range of 600 and 4000 cm^{-1}. Day 0 samples were allowed to gel at 37°C for 4 h in an oven prior to analysis. Day 1 and 7 samples were incubated in 1X PBS (PBS, 10X, Thermo Fisher Scientific, Waltham, MA) at 37°C for 1 and 7 days prior to analysis. The buffer was changed every 2 days. Each hydrogel was washed in deuterated water (D$_2$O) (Sigma-Aldrich, St. Louis, MO) three times for 30 minutes prior to the measurements to remove interference of water in the amide I region (1700–1600 cm^{-1}). Data analysis was performed using the Fourier self-deconvolution method.

LC-MS/MS: Silk hydrogels (1 mL, 2.5 % w/v) of 1, 30 and 120 DT silk were immersed with 1 mL of 12 M hydrochloric acid (HCl, 37%, Sigma-Aldrich, St. Louis, MO) at 60°C for 8h. The hydrolysed samples were dehydrated at 95°C overnight using a digital dry heat bath (Model: BSH1002, USA Scientific, Ocala, FL). The solid samples were then reconstituted in 1 mL of 75% v/v LC-MS grade acetonitrile (Fisher Scientific, Waltham, MA) in LC-MS grade water (Fisher Scientific, Waltham, MA) and then diluted with 75% v/v acetonitrile in water to a final concentration of 400 µg mL^{-1}. LC-MS/MS analysis was performed according to the previously described method[30] to detect dityrosine using an Agilent 1200 series high performance liquid chromatography (HPLC) instrument and an Agilent 6410 triple-quadruple mass spectrometer (Agilent Technologies, Santa Clara, CA) operated in positive electrospray ionization mode. For the analyses, 20 µL samples were injected into a hydrophobic interaction liquid chromatography (HILIC) column (Zorbax HILIC Plus, 4.6 × 100 mm, 3.5 µm, Agilent Technologies, Santa Clara, CA) at 37 °C using a gradient elution method at flow rate of 1 mL/min. The gradient method was as follows: 95:5 acetonitrile to water with 0.1% v/v formic acid for 1 min, increased to 5:95 acetonitrile to water with 0.1% v/v formic acid over 5 min, held for 2 min, and then returned 95:5 acetonitrile to water with 0.1% v/v formic acid. Under these conditions, the typical retention time for dityrosine were 4.8 minute. Product ions for dityrosine (*m/z* transition = 361.1 → 315.3) were identified using a product ion scan, and the collision energy for each analyte was optimized to yield the maximum signal. This information was integrated with a multiple reaction monitoring (MRM) program in the Agilent Mass Hunter Data Acquisition software (Agilent Technologies, Santa Clara, CA). The relative abundance and relative peak area of dityrosine were compared within the sample groups based on the peak areas.

Compression Test: Unconfined compression tests were performed on an Instron 3366 uniaxial tensile testing system (Instron, Norwood, MA). Preformed hydrogels (~8 mm in diameter and ~4 mm in height) were loaded between stainless steel parallel plates. The upper plate was then lowered until a compression force of ~0.002 N was achieved to ensure full contact. A single compressive loading/unloading cycle to 30% strain at 0.667% s^{-1}was then performed. Prior to the test, the hydrogels were incubated in PBS buffer (1x) at 37°C overnight. Compressive modulus was calculated for each sample as the slope between 5% and 10% strain.

Enzymatic *in vitro* degradation: A 200 µL aliquot of silk hydrogel discs of different DTs were prepared in the presence of HRP/H$_2$O$_2$ in PDMS (Polydimethylsiloxane) molds. After 4h, the hydrogels were incubated in 1X PBS at room temperature for 4h. Hydrogel discs were then transferred into 2,000 µL of 0.001 U/mL of chymotrypsin (type XIV from *Streptomyces griseus*, Sigma-Aldrich, St. Louis, MO) dissolved in 1X PBS in 24-well plates. The enzyme buffer solution was changed with fresh solution every 2 days. At every time point, enzyme solution was removed, hydrogels were washed in Ultrapure™ distilled water (Thermo Fisher Scientific, Waltham, MA) over night at room temperature, frozen overnight at -80°C, lyophilized and weighed. Results are reported as residual percentage mass remaining of the initial weight of the hydrogel at day 0 (n = 3).

Swelling ratio and contraction measurement: A 200 µL volume of SF hydrogels of different DT were prepared in PDMS molds for swelling and contraction measurements. After hydrogelation, the hydrogels were weighed to obtain initial weight (W_i). The hydrogels were incubated for 24h in distilled water for swelling and 1X PBS (PBS, 10X, Thermo Fisher Scientific, Waltham, MA) for contraction experiment. At different time intervals, the hydrogels were removed and blotted on paper towels before measuring the final weight (W_f). The percentage swelling and contraction of the hydrogel were calculated by using the following equation.

% swelling (contraction) = (W_f/ W_i) X 100

Cell Survival and Proliferation: Commercial L929 mouse fibroblast cells (ATCC, Manassas, VA) were cultured in growth media composed of Dulbecco's Modified Eagle Medium (DMEM, Gibco) supplemented with 10% fetal bovine serum and 1% penicillin-streptomycin (Life Technologies, Carlsbad, CA). For sterilization, SF solutions were filtered with 0.22 µm syringe filter unit (polyvinylidene difluoride membrane, MillexGV, Millipore). Cells at passage 7 were seeded on the surface of preformed SF hydrogel of different molecular weight (~11 mm in diameter and ~2.5 mm in height) prepared by HRP/H$_2$O$_2$ method and TCP controls at a density of 5,000 cells cm^{-2}. The media was changed every 3 days. The viability of cells was investigated using LIVE/DEAD Cell Imaging Kit (Invitrogen by Thermo Fisher Scientific) after being cultured for 1, 3, and 7 days. Samples were imaged using a BZ-X700 Fluorescence Microscope (Keyence Corp., Itasca, IL). Metabolic activity at days 1, 3, and 7 was determined using Alamar Blue assay by incubating cells in 500 µL dye solution (10% v/v in DMEM high glucose colorless (Gibco) solution) for 2 h at 37°C and 5% CO$_2$. Absorbance was measured at 570 nm (reduced) and 595 nm (oxidized) using a SpectraMax M2 multi-mode microplate reader (Molecular Devices, Sunnyvale, CA). Dye reduction (%) was calculated as described in the assay guidance manual. Blank TCP

and acellular hydrogels were used to adjust for background absorbance.

Statistics –ATR-FTIR, LC-MS/MS, optical transparency, *in vitro* enzymatic degradation, hydrogel swelling and contraction, compression tests were performed on n=3 independent sample replicates at each condition. Biological studies and analysis were carried out on n=4 independent sample replicates for each condition. All data are expressed as means ± standard deviations and used to generate graphical figures. One or two-way analysis of variance (ANOVA) with turkey's post-hoc multiple comparison test was performed using GraphPad prism (GraphPad Software, San Diego, CA) to determine statistical significance (*$p < 0.05$, **$p < 0.01$ and ***$p < 0.001$).

Corresponding Author

Correspondence should be addressed to Prof. David L. Kaplan (david.kaplan@tufts.edu)

Conflicts of interest

The authors declare no conflict of interest.

Acknowledgements

Notes and references

1.   J. Li and D. J. Mooney, *Nature Reviews Materials*, 2016, **1**, 1-17.
2.   N. A. Peppas, *Current opinion in colloid & interface science*, 1997, **2**, 531-537.
3.   O. Hasturk and D. L. Kaplan, *Acta biomaterialia*, 2019, **95**, 3-31.
4.   J. L. Drury and D. J. Mooney, *Biomaterials*, 2003, **24**, 4337-4351.
5.   S. Van Vlierberghe, P. Dubruel and E. Schacht, *Biomacromolecules*, 2011, **12**, 1387-1408.
6.   N. Annabi, A. Tamayol, J. A. Uquillas, M. Akbari, L. E. Bertassoni, C. Cha, G. Camci-Unal, M. R. Dokmeci, N. A. Peppas and A. Khademhosseini, *Advanced materials*, 2014, **26**, 85-124.
7.   B. V. Slaughter, S. S. Khurshid, O. Z. Fisher, A. Khademhosseini and N. A. Peppas, *Advanced materials*, 2009, **21**, 3307-3329.
8.   L. Klouda and A. G. Mikos, *European journal of pharmaceutics and biopharmaceutics*, 2008, **68**, 34-45.
9.   A. S. Hoffman, *Advanced drug delivery reviews*, 2012, **64**, 18-23.
10.   C. B. Highley, G. D. Prestwich and J. A. Burdick, *Current opinion in biotechnology*, 2016, **40**, 35-40.
11.   A. D. Augst, H. J. Kong and D. J. Mooney, *Macromolecular bioscience*, 2006, **6**, 623-633.
12.   S. M. Mithieux, J. E. Rasko and A. S. Weiss, *Biomaterials*, 2004, **25**, 4921-4927.
13.   K. H. Bae, L.-S. Wang and M. Kurisawa, *Journal of Materials Chemistry B*, 2013, **1**, 5371-5388.
14.   N. A. Peppas, J. Z. Hilt, A. Khademhosseini and R. Langer, *Advanced materials*, 2006, **18**, 1345-1360.
15.   M. Floren, C. Migliaresi and A. Motta, *Journal of functional biomaterials*, 2016, **7**, 26.
16.   C. Guo, C. Li and D. L. Kaplan, *Biomacromolecules*, 2020.
17.   S. Kapoor and S. C. Kundu, *Acta biomaterialia*, 2016, **31**, 17-32.
18.   S. Sahoo, C. Chung, S. Khetan and J. A. Burdick, *Biomacromolecules*, 2008, **9**, 1088-1092.
19.   C. Vepari and D. L. Kaplan, *Prog. Polym. Sci.*, 2007, **32**, 991-1007.
20.   G. H. Altman, F. Diaz, C. Jakuba, T. Calabro, R. L. Horan, J. Chen, H. Lu, J. Richmond and D. L. Kaplan, *Biomaterials*, 2003, **24**, 401-416.
21.   Y. Cao and B. Wang, *International journal of molecular sciences*, 2009, **10**, 1514-1524.
22.   B. Kundu, N. E. Kurland, S. Bano, C. Patra, F. B. Engel, V. K. Yadavalli and S. C. Kundu, *Progress in polymer science*, 2014, **39**, 251-267.
23.   T. Yucel, P. Cebe and D. L. Kaplan, *Biophys. J.*, 2009, **97**, 2044-2050.
24.   X. Wang, J. A. Kluge, G. G. Leisk and D. L. Kaplan, *Biomaterials*, 2008, **29**, 1054-1064.
25.   X. Hu, Q. Lu, L. Sun, P. Cebe, X. Wang, X. Zhang and D. L. Kaplan, *Biomacromolecules*, 2010, **11**, 3178-3188.
26.   H. Wu, S. Liu, L. Xiao, X. Dong, Q. Lu and D. L. Kaplan, *ACS applied materials & interfaces*, 2016, **8**, 17118-17126.
27.   U.-J. Kim, J. Park, C. Li, H.-J. Jin, R. Valluzzi and D. L. Kaplan, *Biomacromolecules*, 2004, **5**, 786-792.
28.   M. H. Kim and W. H. Park, *International journal of nanomedicine*, 2016, **11**, 2967.
29.   B. P. Partlow, C. W. Hanna, J. Rnjak-Kovacina, J. E. Moreau, M. B. Applegate, K. A. Burke, B. Marelli, A. N. Mitropoulos, F. G. Omenetto and D. L. Kaplan, *Advanced functional materials*, 2014, **24**, 4615-4624.
30.   M. McGill, J. M. Coburn, B. P. Partlow, X. Mu and D. L. Kaplan, *Acta biomaterialia*, 2017, **63**, 76-84.
31.   J. N. Rodríguez-López, D. J. Lowe, J. Hernández-Ruiz, A. N. Hiner, F. García-Cánovas and R. N. Thorneley, *Journal of the American Chemical Society*, 2001, **123**, 11838-11847.
32.   B. P. Partlow, M. B. Applegate, F. G. Omenetto and D. L. Kaplan, *ACS Biomaterials Science & Engineering*, 2016, **2**, 2108-2121.
33.   N. R. Raia, D. Jia, C. E. Ghezzi, M. Muthukumar and D. L. Kaplan, *Biomaterials*, 2020, **233**, 119729.
34.   N. R. Raia, B. P. Partlow, M. McGill, E. P. Kimmerling, C. E. Ghezzi and D. L. Kaplan, *Biomaterials*, 2017, **131**, 58-67.
35.   O. Hasturk, K. E. Jordan, J. Choi and D. L. Kaplan, *Biomaterials*, 2020, **232**, 119720.
36.   S. Browne, S. Hossainy and K. E. Healy, *ACS Biomaterials Science & Engineering*, 2019.
37.   I. Noh, G.-W. Kim, Y.-J. Choi, M.-S. Kim, Y. Park, K.-B. Lee, I.-S. Kim, S.-J. Hwang and G. Tae, *Biomedical materials*, 2006, **1**, 116.

38. Y. Zhang and C.-C. Chu, *Journal of bioactive and compatible polymers*, 2002, **17**, 65-85.
39. H. J. Kong, D. Kaigler, K. Kim and D. J. Mooney, *Biomacromolecules*, 2004, **5**, 1720-1727.
40. A. P. Tabatabai, B. P. Partlow, N. R. Raia, D. L. Kaplan and D. L. Blair, *Langmuir*, 2018, **34**, 15383-15387.
41. H. Y. Zhou, X. G. Chen, M. Kong, C. S. Liu, D. S. Cha and J. F. Kennedy, *Carbohydrate polymers*, 2008, **73**, 265-273.
42. B. K. Park and I. C. Um, *Int. J. Biol. Macromol.*, 2018, **106**, 1166-1172.
43. H. Kim, D. Song, M. Kim, S. Ryu, I. Um, C. Ki and Y. Park, *Polymer*, 2016, **90**, 26-33.
44. M. Khanmohammadi, M. B. Dastjerdi, A. Ai, A. Ahmadi, A. Godarzi, A. Rahimi and J. Ai, *Biomaterials science*, 2018, **6**, 1286-1298.
45. D. N. Rockwood, R. C. Preda, T. Yücel, X. Wang, M. L. Lovett and D. L. Kaplan, *Nature protocols*, 2011, **6**, 1612.
46. B. P. Partlow, A. P. Tabatabai, G. G. Leisk, P. Cebe, D. L. Blair and D. L. Kaplan, *Macromolecular bioscience*, 2016, **16**, 666-675.
47. L. S. Wray, X. Hu, J. Gallego, I. Georgakoudi, F. G. Omenetto, D. Schmidt and D. L. Kaplan, *Journal of Biomedical Materials Research Part B: Applied Biomaterials*, 2011, **99**, 89-101.
48. M. Gulrajani, *Review of Progress in Coloration and Related Topics*, 1992, **22**, 79-89.
49. C. S. Ki, J. W. Kim, H. J. Oh, K. H. Lee and Y. H. Park, *International journal of biological macromolecules*, 2007, **41**, 346-353.
50. J. H. Lee, D. W. Song, Y. H. Park and I. C. Um, *International journal of biological macromolecules*, 2016, **89**, 273-278.
51. Y. J. Wang and Y. Q. Zhag, 2011.
52. W. L. Stoppel, A. E. Gao, A. M. Greaney, B. P. Partlow, R. C. Bretherton, D. L. Kaplan and L. D. Black III, *Journal of Biomedical Materials Research Part A*, 2016, **104**, 3058-3072.
53. X. Hu, D. Kaplan and P. Cebe, *Macromolecules*, 2006, **39**, 6161-6170.
54. H. J. Cho, C. S. Ki, H. Oh, K. H. Lee and I. C. Um, *Int. J. Biol. Macromol.*, 2012, **51**, 336-341.
55. M. McGill, J. M. Coburn, B. P. Partlow, X. Mu and D. L. Kaplan, *Acta Biomater.*, 2017, **63**, 76-84.
56. A. J. Bailey, J. Macmillan, P. R. Shrewry, A. S. Tatham, J. Gosline, M. Lillie, E. Carrington, P. Guerette, C. Ortlepp and K. Savage, *Phil. Trans. R. Soc. Lond. B*, 2002, **357**, 121-132.
57. J. Fu, *J. Polym. Sci., Part B: Polym. Phys.*, 2018, **56**, 1336-1350.
58. C. Li, C. Guo, V. Fitzpatrick, A. Ibrahim, M. J. Zwierstra, P. Hanna, A. Lechtig, A. Nazarian, S. J. Lin and D. L. Kaplan, *Nature Reviews Materials*, 2019, 1-21.
59. Y. Qiu and K. Park, *Advanced drug delivery reviews*, 2001, **53**, 321-339.
60. T. V. Chirila, S. Suzuki and C. Papolla, *Biotechnology and applied biochemistry*, 2017, **64**, 771-781.
61. K. Trabbic-Carlson, L. A. Setton and A. Chilkoti, *Biomacromolecules*, 2003, **4**, 572-580.
62. S. Gunasekaran, T. Wang and C. Chai, *Journal of applied polymer science*, 2006, **102**, 4665-4671.
63. G. Elyashevich, N. Bel'nikevich and S. Vesnebolotskaya, *Polymer Science Series A*, 2009, **51**, 550-553.
64. L. Zhou, X. Chen, Z. Shao, Y. Huang and D. P. Knight, *The journal of physical chemistry B*, 2005, **109**, 16937-16945.
65. U.-J. Kim, J. Park, H. J. Kim, M. Wada and D. L. Kaplan, *Biomaterials*, 2005, **26**, 2775-2785.
66. Q.-X. Ruan and P. Zhou, *Journal of Molecular Structure*, 2008, **883**, 85-90.
67. E. S. Gil, B. B. Mandal, S.-H. Park, J. K. Marchant, F. G. Omenetto and D. L. Kaplan, *Biomaterials*, 2010, **31**, 8953-8963.
68. A. Matsumoto, J. Chen, A. L. Collette, U.-J. Kim, G. H. Altman, P. Cebe and D. L. Kaplan, *The Journal of Physical Chemistry B*, 2006, **110**, 21630-21638.
69. J. A. Akkara, K. J. Senecal and D. L. Kaplan, *Journal of Polymer Science Part A: Polymer Chemistry*, 1991, **29**, 1561-1574.
70. D. L. Heichel and K. A. Burke, *ACS Biomaterials Science & Engineering*, 2019, **5**, 3246-3259.
71. G. Freddi, A. Anghileri, S. Sampaio, J. Buchert, P. Monti and P. Taddei, *Journal of biotechnology*, 2006, **125**, 281-294.
72. J. Choi, M. McGill, N. R. Raia, O. Hasturk and D. L. Kaplan, *Advanced healthcare materials*, 2019, **8**, 1900644.
73. F. Mijangos, F. Varona and N. Villota, *Environmental science & technology*, 2006, **40**, 5538-5543.
74. L.-S. Wang, J. E. Chung and M. Kurisawa, *Journal of Biomaterials Science, Polymer Edition*, 2012, **23**, 1793-1806.
75. E. Hadjipanayi, V. Mudera and R. Brown, *Journal of tissue engineering and regenerative medicine*, 2009, **3**, 77-84.
76. H. El-Mohri, Y. Wu, S. Mohanty and G. Ghosh, *Materials Science and Engineering: C*, 2017, **74**, 146-151.
77. K. Tsubouchi, Y. Igarashi, Y. Takasu and H. Yamada, *Bioscience, biotechnology, and biochemistry*, 2005, **69**, 403-405.
78. T. V. Chirila, S. Suzuki, L. J. Bray, N. L. Barnett and D. G. Harkin, *Progress in biomaterials*, 2013, **2**, 14.
79. L. Lamboni, M. Gauthier, G. Yang and Q. Wang, *Biotechnology advances*, 2015, **33**, 1855-1867.
80. P. Roach, D. Farrar and C. C. Perry, *Journal of the American Chemical Society*, 2005, **127**, 8168-8173.
81. O. Hasturk, A. Sivas, B. Karasozen, U. Demirci, N. Hasirci and V. Hasirci, *Advanced healthcare materials*, 2016, **5**, 2972-2982.
82. O. Hasturk, M. Ermis, U. Demirci, N. Hasirci and V. Hasirci, *Colloids and Surfaces B: Biointerfaces*, 2019, **178**, 44-55.
83. Y. Arima and H. Iwata, *Biomaterials*, 2007, **28**, 3074-3082.
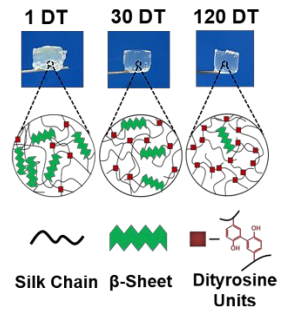
we report a fundamental study on effect of different silk degumming time on biomaterial properties of enzymatically crosslinked hydrogels.